Measurement of the ^{97}Mo(n,γ) reaction with the DANCE γ calorimeter array

C. L. Walker, M. Krtička, B. Baramsai, F. Bečvář, T. A. Bredeweg, A. Chyzh, R. C. Haight, M. Jandel, J. Kroll, G. E. Mitchell, J. M. O'Donnell, R. S. Rundberg, J. L. Ullmann, S. Valenta, and J. B. Wilhelmy

Phys. Rev. C **92**, 014324 — Published 29 July 2015

DOI: 10.1103/PhysRevC.92.014324

Measurement of the ^{97}Mo(n,γ) reaction with the DANCE γ calorimeter array

C.L. Walker,[1,2] M. Krtička,[3,*] B. Baramsai,[1,2] F. Bečvář,[3] T.A. Bredeweg,[2] A. Chyzh,[1] R.C. Haight,[2] M. Jandel,[2] J. Kroll,[3] G.E. Mitchell,[1] J.M. O'Donnell,[2] R.S. Rundberg,[2] J.L. Ullmann,[2] S. Valenta,[3] and J.B. Wilhelmy[2]

[1] *North Carolina State University, Raleigh, NC 27695 and Triangle Universities Nuclear Laboratory, Durham, NC 27708*
[2] *Los Alamos National Laboratory, Los Alamos, New Mexico 87545, USA*
[3] *Faculty of Mathematics and Physics, Charles University in Prague, V Holešovičkách 2, CZ-180 00 Prague 8, Czech Republic*

Spectra of γ rays following the ^{97}Mo(n,γ) reaction were measured as a function of incident neutron energy with the DANCE (Detector for Advanced Neutron Capture Experiments) array of 160 BaF_2 scintillation detectors at the Los Alamos Neutron Science Center using an enriched ^{97}Mo target. These spectra were used for the assignment of spins of the ^{97}Mo resonances up to neutron energy $E_n = 1.7$ keV, as well as in the study of photon strength functions (PSFs) in ^{98}Mo. Analysis of the spectra with the nuclear statistical model showed that they can be well reproduced with the same PSF models which well described the γ decay following slow neutron capture in ^{95}Mo. On the other hand, the spectra are inconsistent with PSFs describing some other experimental data in ^{98}Mo.

PACS numbers: 29.30.Hs, 27.60.+j, 25.40.Lw, 25.40.Ny, 28.20.Np

I. INTRODUCTION

With contemporary experimental techniques complete spectroscopy data on levels in medium- and heavy-mass nuclei, including all quantum characteristics of the levels and interconnecting γ transitions involved, can be obtained only for levels with energies below at most 2 MeV in medium- and heavy-mass nuclei away from closed shells. This represents an obstacle in studying nuclear structure for higher lying states of these nuclei. However, these limitations, originating mainly from the nuclear level density (NLD) rapidly increasing with excitation energy, still allow us to acquire experimental data on average decay rate of the levels, even at an excitation energy region up to the neutron emission threshold, without the need for resolving individual levels. Gamma decay of the nucleus in this, the so-called quasi-continuum region, is believed to be described by the statistical model in terms of the NLD and a set of photon strength functions (PSFs) for individual multipolarities.

The shape of PSFs of Mo isotopes is a puzzle, as existing data on these quantities obtained from different reactions seem in striking disagreement. Data from the (^{3}He,$\alpha\gamma$) and (^{3}He,^{3}He'γ) reactions measured at the Oslo Cyclotron Laboratory indicated a low-energy enhancement of PSFs at energies $E_\gamma \lesssim 3$ MeV for the whole chain of Mo isotopes [1] when compared with conventional models for $E1$ and $M1$ PSFs. The PSF consistent with such a low-energy enhancement was recently reported in ^{95}Mo also from analysis of ^{94}Mo(d,p$\gamma\gamma$) data [2]. There exist theoretical explanations of a low-E_γ enhancement utilizing both $E1$ [3] and $M1$ [4, 5] transitions. However, this enhancement is not supported by the data from two different ^{95}Mo(n,γ) experiments: (i) measurement of the two-step γ cascades (TSCs) following the capture of thermal neutrons using a HPGe detector coincidence setup [6], and (ii) measurement of spectra of the multi-step γ cascades (MSCs) following neutron capture at isolated resonances using the highly segmented BaF_2 Detector for Advanced Neutron Capture Experiments (DANCE) at Los Alamos [7].

There are also several data sets from (γ,γ') measurements in Mo isotopes. Experimental points at $E_\gamma \approx 3.5$ MeV [8] from (γ,γ') agree with data from the ^{3}He-induced reactions; however data from these two reactions at higher E_γ strongly disagree. This disagreement is especially clear when the Oslo data are compared with data measured with the continuous γ source at the ELBE facility in Dresden-Rossendorf [9]; the disagreement is less striking compared with (γ,γ') data measured with a quasi-monoenergetic HIγS beam [10, 11].

To facilitate understanding of these above-mentioned discrepancies in PSFs we undertook a measurement of MSC spectra following the neutron capture at a large number of isolated s- and p- wave resonances of ^{97}Mo. The measurement was undertaken with the DANCE system [12, 13] installed at a beam of the Lujan Neutron Scattering Center at the Los Alamos Neutron Science Center (LANSCE) [14, 15]. Results of our analysis of these spectra with the statistical model are presented in this paper. In general, knowing the PSFs, we can predict the MSC intensity as a function of γ-ray energy for individual γ multiplicities and various J^π of the neutron resonances of interest. Using the Monte Carlo technique all of these multifaceted predictions, based on present knowledge of PSFs from previous experiments, can be obtained and in turn compared with the experimentally observed MSC spectra. With this approach we tested the validity of previous conclusions regarding the PSFs of ^{98}Mo and the validity of the statistical model in general.

As a byproduct, our measurements made it possible to determine spin values for a large number of ^{97}Mo res-

*Corresponding author; Electronic address: krticka@ipnp.troja.mff.cuni.cz

onances. These results are important for calculations in nuclear astrophysics, as well as for the needs of nuclear technologies, in particular those based on the use of uranium-molybdenum fuel.

The paper is organized as follows: the experimental setup is described in Sec. II and simulations with the statistical model in Sec. III. Section IV deals with the determination of resonance spins and parities, while Sec. V lists results of the analysis of MSC spectra. The consistency of our results with other available experimental data is discussed in Secs. VI and VII and the main conclusions are summarized in Sec. VIII.

II. EXPERIMENT AND DATA PROCESSING

A. Experimental details

A four-day long neutron-capture experiment on ^{97}Mo was performed at neutron flight path 14 at LANSCE [14, 15]. Spallation neutrons were produced by irradiation of a tungsten target with 800-MeV protons with a repetition rate of 20 Hz. The low-energy part of the neutron-flux distribution is enhanced by a water-moderator. The experimental approach is similar to that of Sheets *et al.* [7] and only the relevant differences will be reported here.

A self-supporting 20 mg/cm^2 thick 1×1 inch square metal foil sample of Mo enriched in ^{97}Mo to 94.2% was located at the center of the DANCE detector at a distance of 20.25 m from the spallation neutron source. DANCE is a highly-efficient, high granularity γ-ray calorimeter consisting of 160 BaF_2 crystals which cover a solid angle of $\approx 3.5\pi$ with an efficiency of 86% for a single photon with an energy of 1 MeV [16]. A ^{6}LiH shell about 6-cm thick is placed between the sample and the BaF_2 crystals to absorb neutrons that scatter from the sample and would otherwise strike the BaF_2 crystals. The energy of neutrons impinging on the target was determined using the time-of-flight technique.

The DANCE data acquisition system [17] is based on digitization of signals from all 160 detectors using four-channel Acqiris DC-265 digitizers. Use of two channels enables the handling of both the fast and slow components of the signals from the BaF_2 crystals separately with a resolution of 8 bits with a sampling rate of 500 mega samples per second. The yield ratio of the fast to slow components of the signal is used for discrimination against the α background from natural radioactivity of Ra in the BaF_2 crystals [13]. The digitized signals provide information on timing, particle type and absorbed energy for each physical event in the crystals. Data were collected within a time-of-flight interval of 0-500 μs which covers neutron energies $E_n > 8.57$ eV. Only a part of the acquired data, corresponding to $E_n < 1.7$ keV, was used in the present analysis.

The energy calibration of individual DANCE crystals was performed using a combination of γ-ray sources (^{137}Cs, ^{88}Y and ^{22}Na) at low E_γ and the intrinsic radioactivity of the detector material (^{226}Ra). The latter calibration was conducted on a run-by-run basis.

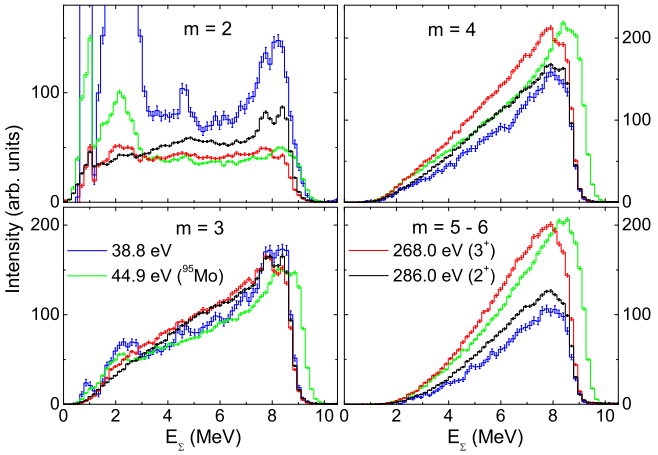

FIG. 1: (Color online) Spectra of energy sums, E_Σ, for three ^{97}Mo resonances, including a previously unknown resonance at 38.8 eV, and a ^{95}Mo contaminant resonance. The cluster multiplicities of the γ cascades, m, and neutron resonance energies are indicated. The spectra are normalized to the intensity of the $m = 3$ spectra in the range 5.5-9.2 MeV.

B. Data reduction

Often an emitted γ ray does not deposit its full energy in a single crystal. Therefore the number of crystals that fire is usually higher than the true multiplicity of a capture event. If all contiguous crystals that fire are combined together to form spatially separated clusters, then to a reasonable approximation the energy deposited in each cluster can be considered as a detector-array response to a single γ ray of a cascade. The number of clusters m observed in an event is referred to as the *cluster multiplicity*.

The cluster multiplicity is much closer to the true multiplicity of the γ cascade than the crystal multiplicity (the total number of crystals that fire) and is used in the analysis. The recorded data were filtered and sorted according to time-of-flight gates, adjusted to cover narrow energy regions in which individual resonances reside, and auxiliary regions between the resonances. As a result, parameters characterizing each filtered event were rewritten into a sequence $\{i, m, E_\gamma^{(1)}, E_\gamma^{(2)}, \ldots, E_\gamma^{(m)}\}$, where i is a label of a neutron energy region, m is a cluster multiplicity and $E_\gamma^{(k)}$ is the k-th cluster energy. From this reduced data set we first constructed the spectra of γ-ray energy sums, E_Σ. Examples are illustrated in Fig. 1.

Each spectrum consists of a *full-energy* peak which is located near the neutron separation energy S_n and a low-energy tail that corresponds to cascades for which part of the emitted γ energy escaped the detection. At low multiplicities the spectra of γ-ray energy sums are strongly

influenced by the background from natural β activity in the BaF_2 crystals for $E_\Sigma \lesssim 3$ MeV.

The full-energy peak in ^{97}Mo is, in fact, a doublet with spacing of about 700 keV. This reflects the level structure of ^{98}Mo, whose first excited level with $J^\pi = 0^+$ at 735 keV does not decay to the ground state via γ emission. A clearly visible shift in position of the full-energy peak in the sum-energy spectrum for the resonance at 44.9 eV, which comes from neutron capture in ^{95}Mo, indicates the possible usefulness of identification of contaminant resonances using the sum-energy spectra.

Figure 1 also shows a clear difference in the multiplicity distribution for s-wave resonances with $J^\pi = 2^+$ and 3^+. This dependence of the multiplicity distribution on resonance spin is exploited in the determination of resonance spins, see Sec. IV.

Only events for which the detected E_Σ is close to the full-energy peak were included in our analysis. Specifically, to construct MSC spectra for individual resonances and various cluster multiplicities m we confined ourselves to values of E_Σ in the range $8.2 - 9.2$ MeV, while for extracting the multiplicity distributions we used a broader range of $5.5 - 9.2$ MeV which helps with the statistics.

A MSC spectrum for multiplicity m was constructed from event-by-event incrementation of counts in the m bins corresponding to m energies $E_\gamma^{(k)}$ deposited in clusters $k = 1, \ldots, m$.

With adjustment of these narrow ranges of E_Σ we could remove a major part of the background. The only background which could affect our analysis was due to capture of neutrons by the barium isotopes in the BaF_2 crystals. This background contribution in the MSC spectra was estimated by two different methods: (i) from MSC spectra obtained with an auxiliary measurement in which the Mo sample was replaced with a natural Fe target for which the cross section is strongly dominated by neutron scattering; the absolute normalization of the background contribution was estimated using the E_Σ region above the full-energy peak or (ii) from the off-resonance regions in the spectra measured with the Mo target under the assumption that the background near the resonance could be considered linear. Both of these background subtraction methods yield corrected spectra which are identical within experimental uncertainties. Moreover, for strong resonances the background contribution in the spectra is negligible.

We also tried to check MSC spectra for E_Σ in the range of $7.45 - 8.05$ MeV – this region corresponds to cascades feeding the first 0^+ excited state and depositing all of their energy in the detector array. But the strongly dominant contribution to these MSC spectra comes from cascades ending at the ground state which do not deposit all the energy in the detector. As evident from comparison of the shape of the sum-energy spectra for ^{95}Mo and ^{97}Mo resonances in Fig. 1, the contribution of cascades ending at the 0^+ excited state in this E_Σ range is only up to about 10%; this value perfectly matches the population of this excited state obtained from simulations. Not surprisingly, the results obtained from analysis of MSC spectra for $E_\Sigma = 7.45 - 8.05$ MeV showed within experimental uncertainties no difference with respect to results from MSC spectra ending at the ground state.

III. SIMULATIONS OF γ-DECAY OF ^{98}Mo

A. Basic Assumptions

To obtain information about the PSFs in ^{98}Mo and also to justify the methods used in determination of resonance spins, we compared different experimental γ-cascade related quantities with the results from simulations based on the nuclear statistical model. The γ decay under different assumptions about the NLD and PSFs was simulated using the DICEBOX algorithm [18] which treats correctly the expected Porter-Thomas fluctuations of individual partial radiation widths [19]. These fluctuations, together with fluctuations expected in the actual number of levels in the nucleus, introduce uncertainties into the γ decay scheme and related γ cascade observables. These uncertainties are accurately treated in the DICEBOX algorithm by constructing different *nuclear realizations*, which are defined by a simulated level scheme and partial radiation widths for transitions between each pair of levels. Typically 50 nuclear realizations, each with 200,000 cascades, were simulated for each initial neutron resonance spin and parity.

The response of the DANCE detector to the generated cascades for each nuclear realization was subsequently obtained with the help of a code based on the GEANT4 package [20].

Several cascade-related quantities can be predicted from the combined DICEBOX+GEANT simulations. Of special interest are MSC spectra, multiplicity distributions in a given E_Σ window, and the total neutron resonance radiation width, Γ_γ.

It should be emphasized that by use of the DICEBOX algorithm we can easily test the degree of agreement between the experimental spectra and different PSF and NLD models, but it is not possible to determine the best model combination. Our procedure is essentially a trial and error approach.

B. Nuclear Level density models

Information on the individual levels of ^{98}Mo up to an excitation energy of 2.5 MeV was taken from available experimental data [21]. For higher excitation energies we used almost exclusively the Back-shifted Fermi Gas (BSFG) NLD model in the form given in Refs. [22, 23]. The energy dependence of the BSFG model is in much better agreement with experimental data obtained from the ^{98}Mo(^{3}He,^{3}He'γ) reaction [24] than is the other often used model, the Constant-temperature (CT) model, see Fig. 2.

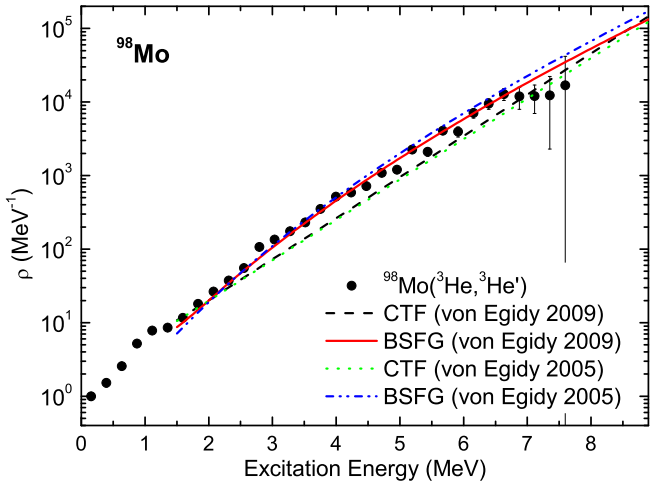

FIG. 2: (Color online) NLD Models for the total level density for all spins up to $J = 10$ and both parities. Experimental points are from the ^{98}Mo(^{3}He,^{3}He'γ) reaction [24].

We considered two different values of the level density parameter a and the back shift energy E_1 from two different NLD parametrizations of von Egidy and Bucurescu [22, 23]: $a = 12.02$ MeV^{-1} and $E_1 = 0.68$ MeV [22], and $a = 11.28$ MeV^{-1} and $E_1 = 0.66$ MeV [23]. The difference between these two parametrizations is due to (i) a different spin dependence of the NLD which is expressed via different values for the spin cut-off parameter and (ii) the introduction of a staggering in the number of levels with even and odd spins at low excitation energies in even-even nuclei. The behavior of the staggering with excitation energy is in question. We used a linear decrease of the size of the staggering effect between 2.5 and 8.5 MeV in simulations with the parametrization from Ref. [23].

Both of these parametrizations are based on an s-wave resonance spacing of $D_0 = 75$ eV [25]. This value differs substantially from the value of $D_0 = 46.5(58)$ eV given in Ref. [26]. The observed number of resonances in ^{97}Mo appears to correspond to the former value, which suggests that the NLD parametrizations used in our simulations are reasonable.

The level density at high excitation energies is expected to be parity independent. However, the parity dependence at low excitation energies remains in question – the available level scheme [21] shows significant parity asymmetry below about 2.5 MeV. We attempted to check the results using a NLD with no asymmetry above 2.5 MeV, as well as for an asymmetry given by the dependence proposed in [27]. The same parameters of the parity dependence function as used in the analysis of MSC spectra of ^{96}Mo were adopted – $\Delta_\pi = 3.2$ MeV and $C_\pi = 1.0$ MeV – see Ref. [7] for details.

C. Photon strength functions

Only electric dipole ($E1$), magnetic dipole ($M1$) and electric quadrupole ($E2$) transitions are considered in our simulations; the influence of $E2$ transitions is expected to be very small.

As our approach is of a trial-and-error character and as there are available PSF data from other experiments – both on ^{98}Mo as well as on neighboring nuclei – we mainly concentrated on evaluation of the acceptability of PSF models that reproduce these available experimental data.

1. *PSFs Reproducing ^{95}Mo(n,γ) data*

Analysis of TSC spectra following thermal neutron capture [6] and of MSC spectra following resonance neutron capture [7] demonstrated that the γ decay of ^{96}Mo can be well described using the model combination given by

$$f(E_\gamma, T) = f_{E1}^{(\mathrm{GLO})} + f_{M1}^{(\mathrm{SF})} + f_{M1}^{(\mathrm{SP})} \qquad (1)$$

for dipole transitions and $f_{E2}^{(\mathrm{SP})}$ for $E2$ transitions. Here $f_{E1}^{(\mathrm{GLO})}$ corresponds to the phenomenological Generalized Lorentzian (GLO) model of the $E1$ PSF [28], $f_{E2}^{(\mathrm{SP})} = 1.2 \times 10^{-12}$ MeV^{-5} to the single particle (SP) model for the $E2$ PSF, $f_{M1}^{(\mathrm{SP})} = 1 \times 10^{-9}$ MeV^{-3} to the SP part of the $M1$ PSF model, and $f_{M1}^{(\mathrm{SF})}$ to the spin-flip (SF) part of the $M1$ PSF model; $f_{M1}^{(\mathrm{SF})}$ was described by a Lorentzian term with values 8.89 MeV, 4.0 MeV and 1.5 mb for the parameters E_{SF} (energy), Γ_{SF} (width), and σ_{SF} (maximum resonance cross section), respectively [25]. The parameter T in Eq. (1) represents the nuclear temperature, as $f_{E1}^{(\mathrm{GLO})}$ depends on T (or equivalently on excitation energy) which implies that the Brink hypothesis [29], which assumes that the PSF is independent of initial and final states and is only a function of E_γ, is not valid in its strict form.

The Lorentzian parameters of the giant electric dipole resonance (GEDR) used in the $f_{E1}^{(\mathrm{GLO})}$ model – energy $E_L = 15.8$ MeV, width $\Gamma_L = 5.94$ MeV, and maximum resonance cross section $\sigma_L = 189$ mb – were based on the photoneutron Saclay measurement [30]. A renormalization of the Saclay measurement by a factor of about 0.86 was suggested for several $A = 88 - 95$ nuclei in Ref. [31]. The applicability of this correction to ^{98}Mo is questionable and has not been considered in our simulations. Recently measured photoneutron data for $E_\gamma < 12$ MeV in ^{98}Mo [32] agree with the Saclay data.

The PSF given by Eq. (1) is shown in Fig. 3. As a result of the T dependence of the $f_{E1}^{(\mathrm{GLO})}$ model, there are different PSFs corresponding to different initial and final level energies. The region occupied by these PSFs is shown in Fig. 3; the lower bound of this region belongs

to transitions to the ground state, $T = 0$, while the upper bound to transitions from the neutron capturing state for which the temperature of the corresponding final level is $T = \sqrt{(S_n - E_\gamma - \Delta)/a}$, where $\Delta = 2.5$ MeV is a pairing shift. All of the other models discussed in this section follow the strict form of the Brink hypothesis, but we also attempted simulations with several other T-dependent models.

We combined the PSFs given by Eq. (1) with several choices of NLD models. The combination with the parity-independent NLD model from the newer parametrization [23] will be referred to as model combination A, the combination with a parity-independent NLD model from the older parametrization [22] as A^*, and the combination with a parity-dependent NLD model from the older parametrization as $A^\dagger$.

To test the necessity of the T-dependence of f_{E1} we also tested several T-independent models based on the GLO parametrization PSF with a "constant temperature". Such a model is often used in descriptions of PSFs derived from Oslo experiments. Model combination E in Fig. 3 represents the total PSF which comes from combination of this f_{E1} with $T = 0.7$ MeV with the same f_{M1}, f_{E2} and NLD models as used in A.

We would like to mention here that theoretical predictions of the $E1$ PSF shape based on thermal excitations coupled to the continuum region [3] seem to be similar to the GLO model with the exception of very low energies. But the temperature T needed for reproduction of Oslo data of ^{98}Mo was very high in these predictions. As there are no available predictions of $E1$ PSF for T corresponding to decay of levels below S_n with this model we have not adopted it in any simulations.

2. *PSFs that reproduce data from ^{3}He-induced reactions*

The PSFs in a series of Mo isotopes have been determined using the so-called *Oslo method* [33] from γ-ray spectra measured at the Oslo cyclotron in ^{3}He-induced reactions; the reaction ^{98}Mo(^{3}He,^{3}He'γ) was used for determination of the PSF in ^{98}Mo [1]. An enhancement of the PSF was observed at low E_γ in all Mo isotopes and a *soft pole* – an extrapolation of PSF toward very low E_γ which diverges at $E_\gamma \to 0$ – was proposed in Ref. [1] as the most probable PSF energy dependence. There were no experimental points from ^{3}He-induced reactions for $E_\gamma < 1$ MeV.

Later, analysis of data from radiative neutron capture on ^{95}Mo [6, 7] clearly showed that the soft pole dependence is unrealistic for a description of PSFs at very low E_γ. Analysis in Refs. [6, 7] also indicated that the maximum allowed PSFs enhancement is given by a weak resonance postulated near $E_\gamma = 1$ MeV that reproduces the Oslo experimental data and gives as small as possible PSFs at very low E_γ.

To confirm these results we performed simulations with a few temperature-independent PSF models which reproduce the Oslo data. Some of these tested models are shown in Fig. 3. Model combination B was obtained from a smoothing of the experimental data over five adjacent points and a constant was used as an approximation for E_γ below the experimental points. The same $M1$ and $E2$ PSFs as for models of the A family were used and the $E1$ part of the combination B corresponded to the difference between the total PSF shown in Fig. 3

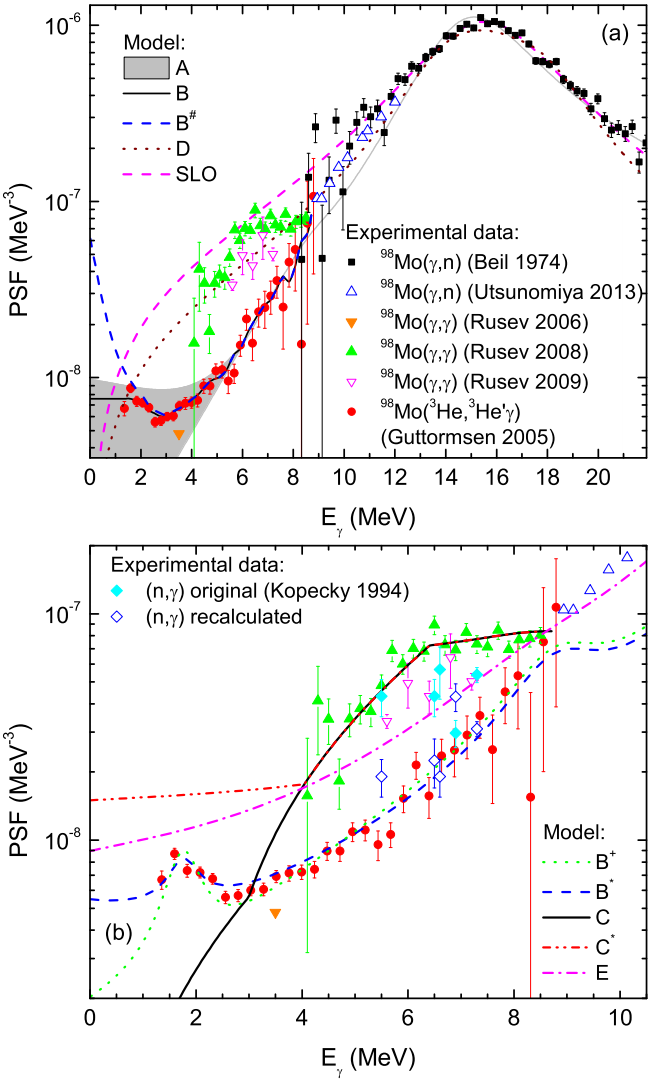

FIG. 3: (Color online) PSFs used in our simulations. The experimental data corresponding to the ^{98}Mo(γ,n) reaction are from (Beil 1974) [30] and (Utsunomiya 2013) [32], the ^{98}Mo(^{3}He,^{3}He'γ) data from (Guttormsen 2005) [1], the ELBE ^{98}Mo(γ,γ') data from (Rusev 2008) [9], the preliminary ^{98}Mo(γ,γ') HIγS data from (Rusev 2009) [10] and the Stuttgart ^{98}Mo(γ,γ') data from (Rusev 2006) [8]. For discussion of the Stuttgart data [8] and data from primary transitions from the (n,γ)reaction, see Sec. VI; the original (n,γ) data are from (Kopecky 1994) [45]. The abbreviations for individual models are also explained in the text. The symbols used for experimental points are the same in both parts of the Figure.

and f_{M1}. Model combinations B^* and $B^\dagger$ correspond to other possible descriptions of the Oslo experimental data. In each of them, the $M1$ PSF consisted of the $f_{M1}^{(SF)}$ and a Lorentzian resonance with a maximum at $E_\gamma = 1.7$ MeV. The $E1$ part of these models is again given by the difference between the total PSF shown in Fig. 3 and the f_{M1}.

An $M1$ low-energy PSF enhancement, which reasonably fits Oslo data at low E_γ in $^{94-96}$Mo isotopes, was recently predicted from shell model calculations [4]. The $M1$ PSF from these calculations can be well described by an exponentially decreasing function of E_γ with very similar parametrization for all three Mo isotopes. For our testing we combined the $M1$ parametrization for ^{96}Mo from [4] with the SF $M1$ model and $E1$ model coming from a fit of Oslo data above $E_\gamma = 2.5$ MeV with a constant PSF at lower E_γ and labeled it as $B^\#$. The same NLD model as for model combination A was used in simulations with all models of the B family.

3. *PSFs deduced from (γ,γ')*

Photon strength functions for $E_\gamma \gtrsim 4$ MeV in a series of even-A Mo isotopes have been reported from (γ,γ') measurements at the ELBE facility in Dresden-Rossendorf [9], where the incoming photons are of bremsstrahlung origin, and their spectrum has a wide energy range. Data from this experiment for ^{98}Mo are also shown in Fig. 3. For testing PSF models which reproduce these (γ,γ') data we adopted several smooth curves which reasonably well describe the data for $E_\gamma > 4$ MeV and tried different extrapolations down to low E_γ within the ranges given by model combinations C and C^* which are shown in Fig. 3.

The discussion in Ref. [9] claims that the measured data in the Mo isotopes are in reasonable agreement with a Lorentzian parametrization of the GEDR, which differs from the parametrization mentioned in Sec. III C 1 and is based on an assumption that Mo nuclei are triaxial [9]. Weak $E1$ strength, which is usually identified with the pygmy dipole resonance (PDR) [34], had to be added to this *Triaxial Lorentzian* (TLO) parametrization in order to describe the data from the ELBE measurement. The TLO parametrization predicts a very different $E1$ PSF shape from the Standard Lorentzian (SLO) for E_γ between about 9 and 13 MeV, but the E_γ dependence of the SLO and TLO model becomes virtually indistinguishable for $E_\gamma \lesssim 8$ MeV apart from the multiplication factor, $f_{E1}^{(\mathrm{SLO})} \cong 1.7 f_{E1}^{(\mathrm{TLO})}$.

Photon scattering on ^{98}Mo for E_γ between about 5.5 and 7.5 MeV was also studied with the mono-energetic photon beam at the HIγS facility. Preliminary results on the the sum of $E1$ and $M1$ PSFs were presented in [10] and are also shown in Fig. 3. These data are in an acceptable agreement with the ELBE data, but they tend to be systematically lower and agree well with the TLO parametrization of f_{E1} with no PDR. We also tested the TLO parametrization for the $E1$ PSF which is a part of the model combination referred to as D. The f_{M1}, f_{E2} and NLD models used in simulations with all models of the C and D family were identical to the models used in model combination A.

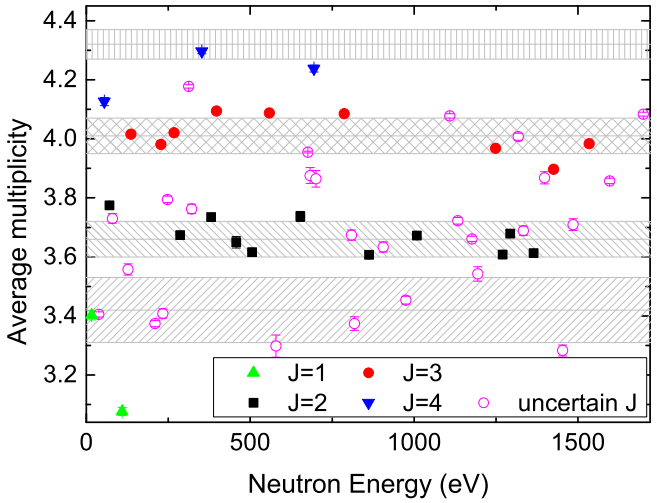

FIG. 4: (Color online) Average multiplicities of well-isolated resonances in ^{97}Mo(n,γ) reaction. Resonances for which we do not assign unique spin in Tab. II are labeled as "uncertain J". Shaded areas correspond to two sigma ranges (average ± one sigma) from prediction of the $\langle m \rangle$ value for 1^-, 2^+, 3^+, and 4^- resonances (from bottom to top) with model combination A, also see Tab. I.

IV. ^{97}Mo RESONANCE SPINS

Several methods which are based on analysis of the experimental multiplicity distribution and the shapes of MSC spectra have been developed for determination of the spin and/or parity of neutron resonances from DANCE data.

A. Average multiplicity and shape of MSC spectra

In the analysis of ^{94,95}Mo(n,γ) reactions the combination of average multiplicity $\langle m \rangle$ with the shape of MSC spectra for $M = 2$ was used [35]. The values of $\langle m \rangle$ of well-separated ^{97}Mo resonances are shown in Fig. 4; multiplicities $m = 2-7$ were used. Resonances for which the spin can be uniquely assigned are highlighted. The $\langle m \rangle$ values of the strongest resonances nicely separate into two groups. These resonances come from s-wave neutron capture and have $J^\pi = 2^+$ (black squares) and 3^+ (red circles). In addition to these two groups, there are also resonances with much higher and much lower $\langle m \rangle$ values. This situation seems to be similar to the ^{95}Mo(n,γ) data where we also observed concentration of the $\langle m \rangle$ values into four groups. In ^{95}Mo the $\langle m \rangle$ was very similar for

TABLE I: Average multiplicities $\langle m \rangle$ of spectra from resonances with different initial spins and parities obtained from simulations with different PSF models.

Model	Average multiplicity $\langle m \rangle$					
	2^+	3^+	1^-	2^-	3^-	4^-
A	3.66(6)	4.01(6)	3.42(11)	3.64(8)	3.94(8)	4.32(5)
A^*	3.68(7)	3.96(14)	3.39(9)	3.58(11)	3.97(7)	4.32(6)
$A^\dagger$	3.62(8)	4.02(7)	3.34(11)	3.63(5)	3.90(8)	4.32(4)
B	3.77(5)	4.02(9)	3.47(14)	3.76(12)	4.01(9)	4.37(8)
B^*	3.73(7)	3.97(11)	3.54(13)	3.79(12)	4.04(9)	4.38(7)
$B^\dagger$	3.68(7)	3.92(11)	3.45(14)	3.70(11)	3.95(10)	4.29(7)
$B^\#$	3.89(6)	4.23(7)	3.60(17)	3.89(18)	4.17(15)	4.58(12)
C	3.29(4)	3.61(5)	3.11(10)	3.27(9)	3.54(9)	3.89(7)
C^*	3.67(5)	3.98(6)	3.30(13)	3.54(12)	3.82(11)	4.20(9)
D	3.55(6)	3.90(5)	3.38(12)	3.63(12)	3.86(7)	4.23(6)
E	3.71(4)	4.00(7)	3.48(13)	3.73(12)	4.00(10)	4.34(8)

resonances with $J^\pi = 2^+$ and 3^- and also for $J^\pi = 3^+$ and 4^- resonances [35]. This experimental finding was supported by results from simulations. The inspection of spectral shapes of $m = 2$ MSC spectra in the ^{95}Mo data permitted the determination of the parity of majority of resonances belonging to the same average-multiplicity group.

In ^{97}Mo the situation seems to be different. Spectra from all resonances with $\langle m \rangle \lesssim 3.8$ show a bump-like structure in the middle of $m = 2$ MSC spectra, which is missing in all resonances with higher $\langle m \rangle$. The bump is expected to be present in MSC spectra from $J = 1$ and 2 resonances and its absence in the MSC spectra from $J = 3$ and 4 resonances is caused by the impossibility of reaching the 0^+ ground state via two dipole γ-rays.

This observation suggests that the grouping of resonances according to $\langle m \rangle$ in ^{97}Mo differs from ^{95}Mo and that $\langle m \rangle$ depends only on the resonance spin in ^{97}Mo. Simulations of $\langle m \rangle$ with different PSFs and NLD model combinations are consistent with this interpretation, see Tab. I. The predictions for $\langle m \rangle$ for 2^+, 3^+, 1^-, and 4^- resonances for model combination A are also plotted in Fig. 4. As is evident, the agreement between experiment and simulations with this model is very good.

As a result, the average multiplicity and the shape of $m = 2$ spectra do not allow identification of the resonance parity in ^{97}Mo. In practice, the applicability of $\langle m \rangle$ is limited to well-resolved resonances and the shape of the MSC spectra to the strong ones.

B. Decomposition of multiplicity distribution into prototypes

The spin determination method proposed in Ref. [36] is based on decomposition of the capture yield, measured as a function of neutron energy, into components that belong to the individual neutron capturing state J^π assignments. It is assumed that each such component displays its own, the so-called "prototypical" multiplicity distribution.

It works very well provided that (i) only two spin-parity sets of resonances are in play, and (ii) the multiplicity distribution for each set does not change with neutron energy. Conditions close to these ideal ones are valid for low-energy resonances of rare earth nuclei

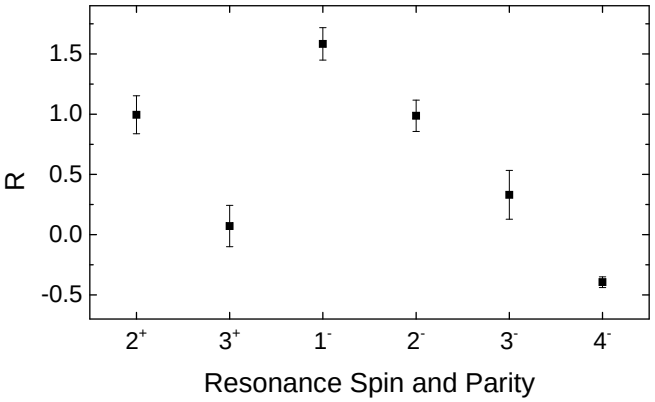

FIG. 5: Ratio R of the $J^\pi = 2^+$ yield with respect to the total yield for various resonance spins and parities, as obtained from DICEBOX/GEANT simulations with model combination A. The error bars correspond to the rms Porter-Thomas uncertainties of R.

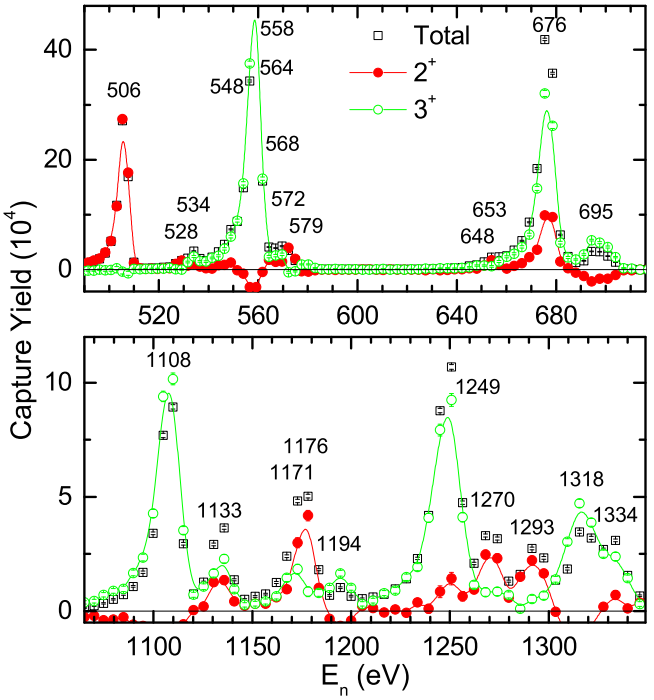

FIG. 6: (Color online) Squares: total capture yield as a function of neutron energy. Full and empty circles: its $J^\pi = 2^+$ and $J^\pi = 3^+$ components respectively. Smooth curves: B-spline fits of the decomposed yields. The resonance energies are indicated.

[36, 37]. In ^{97}Mo(n,γ) the use of this method faces two problems: (i) more prototypical multiplicity distributions are expected due to the presence of p-wave resonances at very low neutron energies, and (ii) the shape and size of the multiplicity distributions for resonances of the same spin-parity group might display unacceptably large fluctuations.

Regarding the first problem, there could be up to six different multiplicity distribution groups in ^{97}Mo(n,γ), although distributions from resonances with different spin and/or parity can be very similar. From the discussion in Sec. IV A we might expect similar distributions for resonances with the same spin independently of their parity. The least-square fit option of the decomposition method from [36] allows its simple generalization for more prototypes. However, the number of different multiplicity distributions in our case would already be comparable to or would even exceed the dimension of the multiplicity space which is used in the fitting procedure. The results of the fitting procedure are very unstable in such case and generalization of the method in this direction does not appear to be working.

Instead we tried to decompose the experimental yield into contributions of two different prototypes in the same way as demonstrated in Ref. [36]. If there is a resonance with multiplicity distribution which differs from both prototypes, neither of two decomposed yields will not correspond to the experimental yield anymore. The original intent of the decomposition made in Ref. [36] is lost, but the method will still serve as a very good identifier of resonance spin and/or parity. In practice the expected multiplicity distribution from 1^- resonances is shifted toward lower multiplicities with respect to $J = 2$ resonances and the distribution from 4^- resonances toward higher multiplicities with respect to $J = 3$ resonances. Using prototypes from known 2^+ and 3^+ resonances the decomposed yield for 1^- and 4^- resonances should be significantly negative for prototypes corresponding to 3^+ and 2^+, respectively. As seen from Fig. 5, the combined DICEBOX + GEANT simulations with a realistic PSFs and NLD model combination A confirm this expectation. The figure shows the simulated ratio R of the 2^+ yield with respect to the total yield.

Simulated ratios R in Fig. 5 also indicate the solution to the second of the above mentioned problems. Simulations indicate that fluctuations of the expected yield of a resonances with given J^π, which are represented by fluctuations of R, are slightly higher in ^{97}Mo than in the rare-earth region, but should still allow reasonable identification or restriction of the resonance spin. The simulations also predict very similar behavior of decomposed yields for resonances with the same spin but opposite parity.

Results of the spin decomposition for two regions of neutron energy are shown in Fig. 6. Prototypical multiplicity distributions were taken from the 286 eV (2^+) and 397 eV (3^+) resonances. The method provides information about the spin even for not well-isolated resonances if they have different multiplicity distributions, see e.g. the results of decomposition for two resonances at $E_n \approx 1175$ eV in Fig. 6.

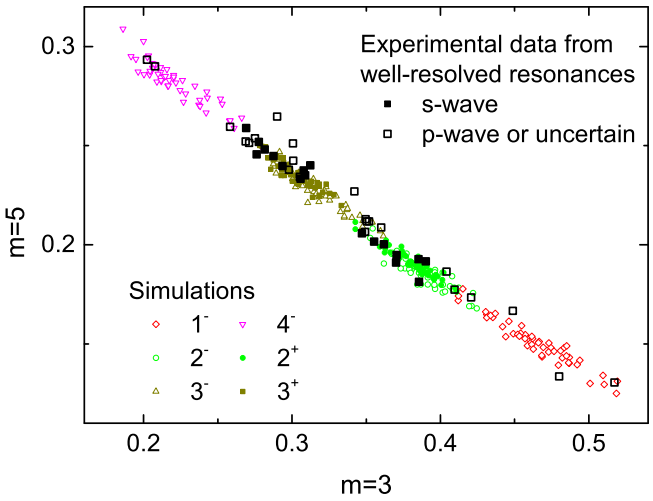

FIG. 7: (Color online) Normalized yield for multiplicity $m = 5$ with respect to $m = 3$ for well-separated resonances in ^{97}Mo(nγ) reaction. The normalization was made with respect to $m = 3 - 6$. The simulated values are from 30 independent nuclear realizations for each resonance spin and parity using model combination A. Experimental uncertainties are not shown in order to make the figure readable. Typical uncertainties are on the level of 10% and make all experimental points fully consistent with the band predicted from simulations.

C. Pattern recognition method

Another possible method for spin/parity assignment of well-separated resonances applicable to DANCE data was introduced in Ref. [38] and named the *pattern recognition method*. This method exploits the fact that resonances with the same spin should create separated "clouds" in the multiplicity-distribution space. The method becomes powerful if the number of resonances is large, but the separation of the clouds in multiplicity space is not easy with a restricted number of resonances which is our case.

However, we can still use this method for restricting the resonance spin. In Fig. 7 we show the relation of intensity in multiplicity $m = 5$ with respect to $m = 3$ for well-resolved resonances. The intensities for different multiplicities were obtained by normalization with respect to total intensity in $m = 3-6$ range. Resonances in the upper left corner are expected to have $J = 4$ while resonances in the lower right corner $J = 1$. Predictions with model combination A from 30 different nuclear realizations for each resonance spin and parity are plotted together with experimental data. There are two well-separated groups of s-wave resonances; this agrees well with predictions of the simulations for $J^\pi = 2^+$ and 3^+.

This result gives us confidence not only in the spin assignments for strong resonances, but also indicates that model combination A reasonably describes many other observables. As in the case of $\langle m \rangle$ the method is applicable only to well-separated resonances.

D. Results on resonance spins

The spin assignments of individual resonances were obtained by combining results from all of the above-mentioned methods for $E_n < 1.7$ keV. These results are presented in Tab. II. We also still see clearly resonances for higher E_n, at least up to $E_n \approx 2$ keV, but as the resolving power of the DANCE measurement significantly decreases with neutron energy the separation of the resonances and the spin assignment becomes rather difficult at $E_n > 1.7$ keV. The resonance spin was assigned uniquely only if all methods gave consistent results. This was the case for approximately one half of the resonances. We were conservative in spin assignments and listed all spins which cannot be completely rejected.

Prior to our measurement information on the resonance spins and parities was available only for strong resonances which were assumed to be s-wave. The parity assignment for weaker resonances in [26] is uncertain and is estimated from the strength of the resonance. The spins of these resonances in JEFF-3.2 [39] and JENDL-4.0 [40] compilations were assigned randomly.

All resonances listed in Ref. [26] are visible in our data. In addition several new resonances have been observed. All of these new resonances are weak. It is not easy to determine neutron widths Γ_n and total radiation widths Γ_γ of the new resonances from our measurement as we do not know precisely the neutron flux. However, we could determine their capture areas A_γ relatively to areas of weak neighboring resonances with known neutron widths. Assuming that A_γ is proportional to $g\Gamma_n$, where g is the statistical spin factor, for weak resonances with $\Gamma_n \ll \Gamma_\gamma$ we obtained values of $2g\Gamma_n$ for all newly observed resonances which are listed in Tab. II. Resonances at 457.3 and 458. 6 eV as well as resonances at 1171.0 and 1176.4 eV form unresolved doublets. Neutron widths for newly observed resonances in these doublets were determined using the decomposition method described in Sec. IV B. Decreasing resolution power might leave some weak resonances for $E_n \gtrsim 1.3$ keV unobserved.

Resonance energies cannot be determined from the DANCE measurement with a precision comparable to that in the literature in the investigated region. Therefore the resonance energies in Tab. II are taken from [26] unless indicated otherwise.

Three resonance regions deserve comment. Decomposition of the resonance at 676.3 eV into prototypes does not indicate any doublet and is reasonably consistent with $J = 3$ – experimental $R \approx 0.25$. The same spin assignment is also consistent with the $\langle m \rangle$ and pattern recognition methods. However, the shape of $m = 2$ MSC spectrum clearly indicates the presence of a resonance with $J = 1$ or 2. We do not see the same intensity in the middle of the $m = 2$ MSC spectrum for any other resonance with $J = 3$ which agrees with expectation from simulations. We propose a close resonance doublet, probably with spins $J = 4$ and $J = 1$ or 2, with a separation less than 3 eV.

Decomposition of the resonance region near 905.7 eV into prototypes gives almost exactly the same yield for 2^+ and 3^+ prototypes. In addition, there seems to be a small energy shift in the maximums of the two prototype yields – the maximum corresponding to 2^+ prototype yield seems to shifted by about 2 eV to lower E_n. Unfortunately, the MSC spectra suffer from poor statistics in this case.

Decomposition of 1133.4 eV resonance into prototypes yields $R \approx 0.4$; average multiplicity and pattern recognition methods are consistent with $J = 2$, but the shape of MSC spectra indicates $J = 3, 4$. A possible doublet would be separated by less than about 3 eV.

V. ANALYSIS OF MSC SPECTRA

The simulated MSC spectra for individual nuclear realizations and a fixed combination of PSF and LD models differ from each other statistically. This is an artifact of the adopted paradigm for the compound nucleus. To characterize these fluctuations, the simulated MSC spectra shown in this paper are plotted in the form of shaded areas, the widths of which correspond to the standard confidence region of spectral intensity, i.e., to its average $\pm\sigma$, usually obtained from 50 independent nuclear realizations. These spectral fluctuations arise from inherent, irreducible statistical uncertainties in the excitation energies of all bound levels involved, uncertainties in branching intensities responsible for depopulation of these levels, and the dominant uncertainties in the intensities of primary transitions depopulating the individual neutron resonances.

Only one common normalization coefficient is sufficient to normalize the simulated and experimental MSC spectra to the same units for all multiplicities. We normalized all of the presented spectra to the same number of counts in the $m = 4$ MSC spectrum. To minimize statistical uncertainties in the experimental data, as well as uncertainties from the simulations, the spectra were binned into coarse bins with a width of 300 keV, which led to some insignificant smearing of the MSC spectra.

To quantify the degree of agreement between the simulated and experimental MSC spectra, extremely time-consuming simulations would be needed as the contents of the individual bins in the MSC spectra are mutually correlated in a complicated fashion and the corresponding correlation matrix is not known *a priori*. As a consequence, the degree of agreement was only checked visually.

As discussed in the previous section we are not able to

TABLE II: Parameters of resonances in the ^{97}Mo(n,γ) reaction. Neutron widths $2g\Gamma_n$ are from Ref. [26] except noted.

E_n (eV)	$2g\Gamma_n$ (meV)	J^π Ref. [26]	J^π Our	Comment	E_n (eV)	$2g\Gamma_n$ (meV)	J^π Ref. [26]	J^π Our	Comment
16.2(1)	0.0026[a]		1		653.2(5)	2.7(3)	(-)	2	
38.8(1)	0.07(2)[b]		2(1)	New	676.3(5)	385(50)	3^+	(4)&(1,2)	See text
55.3(1)	0.035[a]		4		694.7(5)	12.5(8)	(-)	4	
70.92(3)	16.8(15)	2^+	2		700.7(6)	9.3(6)	(-)	(3,4)	
79.55(4)	0.11(2)	(-)	3(2)		786.5(6)	470(66)	3^+	3	
109.58(5)	0.22(8)	(-)	1		809.2(7)	4.0(5)	(-)	(3,4)	
126.89(6)	0.20(8)	(-)	3(2)		818.0(10)	7.5(15)[b]		(1,2)	New
136.32(8)	1.2(1)	(-)	3		862.5(7)	51.6(110)	2^+	2	
209.98(10)	1.10(12)	(-)	1(2)		905.7(8)	10.0(8)	(-)	(2)&(3)	See text
217.0(4)	0.25(8)[b]		(2)	New	975.1(8)	14.2(12)	(-)	2	
227.58(10)	2.4(2)	3(-)	3		1008.2(9)	70(10)	(+)	2	
233.33(10)	0.66(1)	(-)	2(1)		1108.7(10)	280(34)	2^+	3(4)	
247.91(10)	1.6(2)	(-)	3(2)		1133.4(11)	61.2(120)	2(+)	3(2)	See text
268.02(10)	17.0(15)	3^+	3		1171.0(20)	30(10)[b]		(3)	New
286.03(10)	60.0(60)	2^+	2		1176.4(11)	91(10)	(+)	2	
312.1(2)	10.0(15)	3^+	4(3)		1194.2(11)	9.5(10)	(-)	3(4)	
321.1(2)	1.9(2)	(-)	3(2)		1248.8(12)	530(190)	3^+	3	
352.7(2)	9.0(10)	(-)	4		1270.4(13)	58.6(100)	(+)	2	
380.9(2)	6.0(10)	(-)	2		1293.1(13)	43.5(64)	(+)	2	
397.2(2)	75.0(80)	3^+	3		1317.6(13)	64.3(132)	(+)	4(3)	
416.3(5)	0.8(2)[b]		(2)	New	1333.5(13)	55.0(116)	(-)	3(2)	
457.3(3)	1.7(2)	(-)	3		1364.3(14)	76(12)	(+)	2	
458.6(5)	0.7(3)[b]		(2)	New	1375.4(14)	11.4(16)	(-)	(3)	
505.5(3)	62.0(50)	(+)	2		1398.0(14)	14.0(14)	(-)	(2)	
528.3(3)	1.5(2)	(-)	2(1)		1425.2(14)	130(9)	(+)	3	
533.8(4)	4.5(4)	(-)	3		1453.1(14)	18.8(24)	(-)	1(2)	
548.3(4)	4.5(5)	(-)	(1,2)		1485.0(15)	11.8(14)	(-)	3(4)	
558.4(4)	600(50)	3^+	3		1534.2(15)	415(160)	(+)	3	
564.1(4)	2.6(13)	(-)	(1,2)		1554.2(16)	11.4(16)	(-)	(2)	
568.0(4)	6.7(8)	(-)	(3,4)		1596.4(9)	180(30)	(3+)	3	
572.0(4)	5.6(8)	(-)	2(1)		1628.4(16)	14.4(16)	(-)	3(4)	
578.5(4)	1.7(2)	(-)	4(3)		1699.0(17)	134(25)	(+)	4(3)	
648.0(10)	1.3(3)[b]		(3)	New					

[a] Resonances not reported in Ref. [26] but assigned to ^{97}Mo in JEFF3.2 [39] and JENDL4.0 [40]

[b] Neutron width of previously unobserved resonance. See text for description of its determination.

unambiguously assign parity to neutron resonances due to the similarity of different observables – including the spectral shapes of MSC spectra – for resonances with the same spin and opposite parity. This similarity in observables was confirmed with simulations. Unambiguous spin and parity assignment seems to be possible only for several strongest s-wave 2^+ and 3^+ resonances and for some of the 1^- and 4^- resonances which show a very different decay pattern from $J = 2$ and 3 resonances.

Experimental MSC spectra originating from decay of resonances with these J^πs are compared with predictions of simulations with model combination A in Fig. 8. The agreement between simulations and experiment is good for all resonance J^πs. This agreement indicates that the model which was able to describe the TSC and MSC spectra in ^{96}Mo also provides a good description of the γ decay of ^{98}Mo resonances. The consistency in results for two neighboring nuclei might be important for nuclei where no experimental information on the PSFs is available. The simulated MSC spectra for model combinations A^* and $A^\dagger$ are very similar to the spectra from combination A, as shown in Fig. 8. This suggests that our conclusions are not sensitive to the details of the parametrization of the NLD.

The most pronounced difference between experiment and simulations is seen in the $m = 2$ MSC spectrum from

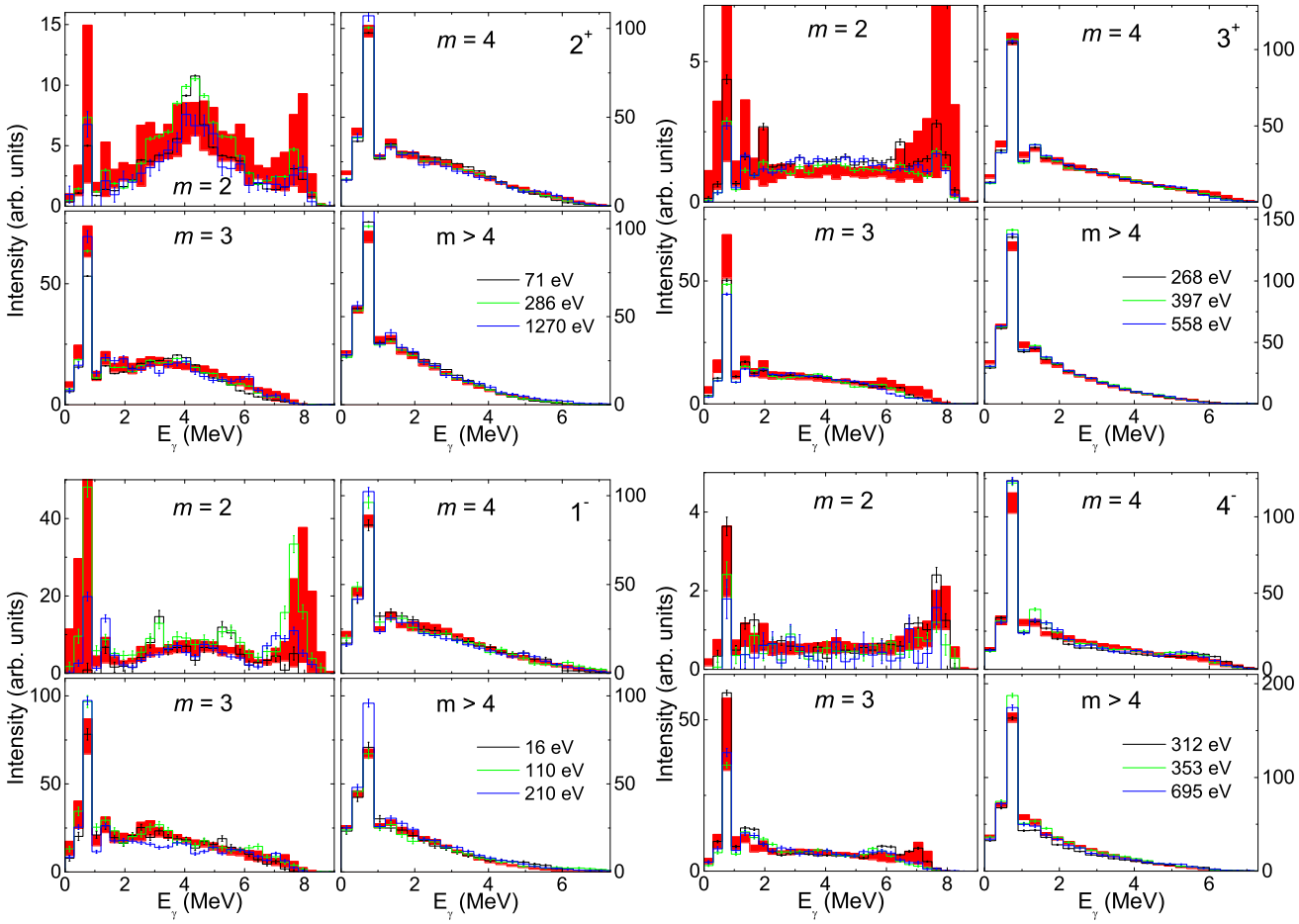

FIG. 8: (Color online) Comparison of simulated MSC spectra using model combination A (shaded regions) with the experimental data for selected resonances (histograms). Resonance energies, spins and parities are indicated.

$J^\pi = 1^-$ resonances, where experimental data show a strong TSC cascade formed by $E_\gamma \approx 3.1$ and 5.3 MeV transitions. This cascade might be a consequence of "non-statistical" effects observed in p-wave neutron capture in Mo isotopes [41–43]. As the cascade intensity does not correlate with the reduced p-wave neutron widths, the valence capture mechanism [41] cannot account for this anomaly, while in principle the doorway mechanism [42] can. Simulations with model combination $A^\dagger$, i.e., with a parity-dependent NLD at low excitation energies, predict larger fluctuations in the $m = 2$ spectrum for 1^- resonances than simulations with model A. As a result the observed intensity of the above-mentioned cascade seems to be quite consistent with simulations within the statistical model for $A^\dagger$ combination.

In any case the possible presence of non-statistical effects in neutron capture in ^{97}Mo is expected to be small as it could enhance only a small fraction of primary transitions from some resonances and should not affect the overall behavior observed in our DANCE experiment. This expectation is consistent with the observation that differences of experimental MSC spectra from different resonances seem to be very similar to fluctuations among them predicted by simulations using the statistical model. This is also in accord with conclusions made from analysis of TSC [6] and MSC spectra [7] in ^{96}Mo and indicates that the statistical model can be used for the description of γ decay following radiative neutron capture in even-even nuclei in this mass region.

The T-dependence of f_{E1} is probably not necessary for description of γ decay from radiative neutron capture. The reproduction of experimental MSC spectra using model E with $T = 0.5 - 0.8$ MeV is only slightly worse compared to that with the model combination A.

None of the T-independent PSFs which describes well the strength observed from ^{3}He-induced photon production at $E_\gamma \lesssim 4$ MeV (model combinations B, B^*, $B^\dagger$ and $B^\#$) is able to reproduce the spectral shapes in $m = 2-4$ MSC spectra. The strongest disagreement is visible in $m = 3$ spectra and is illustrated in Fig. 9 for spectra from positive-parity resonances using model combination B; spectral shapes for B^*, $B^\dagger$, and $B^\#$ are very similar. The intensity of transitions with $E_\gamma = 3 - 5$ MeV is strongly suppressed with respect to other E_γ in predictions of all these model combinations. The enhancement in the model combination $B^\#$ is that strong that also the

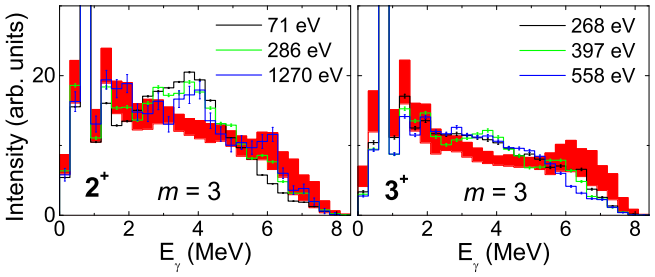

FIG. 9: (Color online) Comparison of predicted MSC spectra with model combination B (shaded area) with experimental MSC spectra (histograms) for $m = 3$ from positive-parity resonances. Resonance energies are indicated.

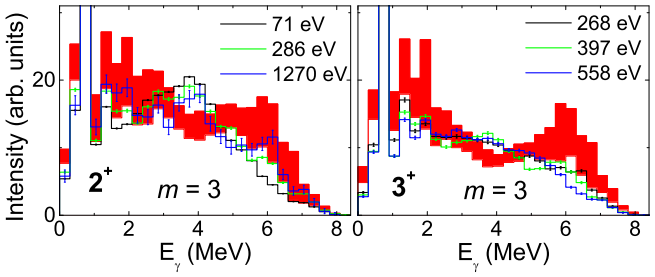

FIG. 10: (Color online) Comparison of predicted MSC spectra with model combination C^* (shaded area) with experimental MSC spectra (histograms) for $m = 3$ from positive-parity resonances. Resonance energies are indicated.

predicted multiplicity distribution is shifted significantly to too high values, see Tab. I. We also tried to lower the size of the $M1$ enhancement in the model combination $B^{\#}$ to get an acceptable agreement with experimental MSC spectra. We found that an allowed enhancement is at least an order of magnitude smaller compared to that proposed in [4] and shown in Fig. 3(a).

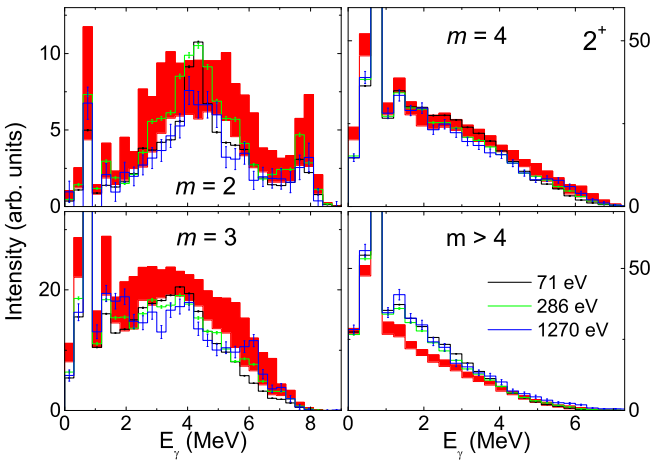

FIG. 11: (Color online) The same as in Fig. 8 but for predictions with model D. Only MSC spectra for 2^+ resonances are compared. Resonance energies are indicated.

We met difficulties in reproducing experimental MSC spectra with any of the model combinations reproducing the Dresden (γ,γ') data (model combinations C and C^*). If a model combination where PSF goes to zero at $E_\gamma \to 0$ (model combination C) is used, the multiplicity distribution is significantly shifted toward lower values. This shift in multiplicity arises from a strong preference of high-energy transitions in model combination C. To obtain a realistic multiplicity distribution we need a PSF which is strongly enhanced with respect to that used in C at $E_\gamma \lesssim 4$ MeV – the E_γ dependence of PSF similar to that used in model combination C^* seems to be required, see also Tab. I. However, as illustrated in Fig. 10 the spectral shape of MSC spectra with model C^*does not seem to be acceptable due to the presence of a too strong bump near $E_\gamma = 6$ MeV.

The multiplicity distribution predicted from simulations with model combination D is also shifted toward lower values, see Fig. 11 and Tab. I. This feature disqualifies the Lorentzian shape of the PSF model, although predicted spectral shapes for individual MSC spectra in this case are not very different from predictions of combination A.

In conclusion, analysis of spectral shapes and multiplicity distributions of MSC spectra indicates that the existence of any pronounced resonance-like structures in PSFs observed previously near energies 2 and 6 MeV from the ^{3}He-induced reaction [1] and the Dresden (γ,γ') measurement [9], respectively, disagrees with our data. However, we cannot reject a presence of much weaker resonance structures in a PSF at these energies. Similarly, an existence of the $M1$ low-energy PSF enhancement of the size predicted in [4] strongly disagrees with our data – a possible enhancement would need to be an order of magnitude lower. This finding perfectly matches our conclusions on PSFs from ^{95}Mo(n,γ) [6, 7]. As ^{98}Mo is expected to be more deformed than ^{96}Mo [25] the $M1$ scissors-mode resonance [44] at $E_\gamma = 2.5-4.0$ MeV might play some role. But our data indicate no or an extremely weak contribution of this resonance. At any rate, a realistic $E1$ PSF model should definitely be less steep than the SLO model at energies $E_\gamma \lesssim 4$ MeV.

VI. COMPARISON WITH OTHER DATA

The agreement between experimental MSC spectra and their predicted counterparts based on PSF models reproducing data from ^{3}He-induced reaction and from (γ,γ') reaction at $E_\gamma \gtrsim 4$ MeV was discussed in the previous section. There are several additional data on PSFs in the Mo region with which our results can be compare.

A. (γ,γ') at low energies

In addition to the ^{98}Mo(γ,γ') data from the ELBE and HIγS facilities, which show the E_γ dependence of

Model	Total radiation width (meV)					
	2^+	3^+	1^-	2^-	3^-	4^-
A	107(5)	112(5)	143(17)	111(5)	114(5)	99(4)
A^*	104(4)	102(4)	121(11)	109(7)	104(4)	98(5)
$A^\dagger$	101(5)	96(4)	130(9)	113(4)	114(4)	102(4)
B	84(4)	87(4)	112(17)	86(4)	90(4)	78(4)
B^*	84(4)	87(3)	109(11)	86(4)	90(4)	77(4)
$B^\dagger$	78(4)	81(4)	103(13)	80(4)	84(4)	72(4)
$B^\#$	80(4)	86(4)	113(13)	83(4)	89(4)	75(3)
C	129(13)	135(13)	195(33)	142(13)	151(15)	119(12)
C^*	272(16)	282(17)	389(59)	292(20)	306(21)	256(16)
D	224(13)	232(13)	315(38)	243(20)	255(16)	210(13)
E	159(8)	166(7)	212(25)	166(8)	174(9)	150(8)

TABLE III: Simulated total radiation width of resonances for all considered model combinations. Uncertainties correspond to the rms deviation predicted by DICEBOX. Experimental values of Γ_γ for s-wave resonances is $\Gamma_\gamma^{(exp)} = 130(20)$ meV [26].

the PSFs for $E_\gamma > 4$ MeV, there also are (γ,γ') data from measurement at energies up to 3.8 MeV using a bremsstrahlung photon beam at Stuttgart[8]. Five dipole transitions were observed for E_γ between 3.25 and 3.75 MeV with $f_{NRF}^{(exp)} = 4.8(2) \times 10^{-9}$ MeV^{-3} assuming that the transition intensities are averaged over a 0.5 MeV wide interval. This value is shown in Fig. 3.

This experimental point is well below the sum of $E1$ and $M1$ PSFs used in model combinations of B, C, D and E families. For the T-dependent $E1$ PSF incorporated in combination A, the lower bound of the range plotted in Fig. 3(a) – which corresponds to PSFs governing transitions from the (γ,γ') reaction – seems to be in very good agreement with $f_{NRF}^{(exp)}$.

The low density of states at low excitation energies implies fluctuations in the observed strength which might allow compatibility with other tested models. But similar values of the observed strength in all even-mass Mo nuclei (with the exception of the lightest ^{92}Mo) [8] at $E_\gamma < 4$ MeV indicate that a realistic PSF model should reasonably reproduce the $f_{NRF}^{(exp)}$ value given in Fig. 3.

B. Total radiation width

Simulated values of Γ_γ for the model combinations described in Sec. III are listed in Tab. III. Values of Γ_γ for different model combinations of the A family indicate that the dependence of Γ_γ on the exact parametrization of a given NLD model – BSFG in this case – is very weak.

On the other hand, the use of a different energy dependence of the NLD would produce significantly different values of Γ_γ. For instance, use of the CT model reduces Γ_γ by a factor of about 1.7 with respect to the BSFG model for the same set of PSF models; the reduction factor slightly depends on the PSF models used. All of the following reasoning related to Γ_γ is valid if (i) the energy dependence of the actual NLD is similar to the BSFG model, (ii) the actual resonance spacing corresponds to the value from [26], and (iii) the experimental value of $\Gamma_\gamma^{(exp)}$ is close to the average value given in [26].

All PSF data obtained from analysis of the ^{3}He-induced reactions on Mo were, in fact, normalized to $\Gamma_\gamma^{(exp)}$. There is a significant difference between the PSF shapes used for the original normalization of PSF experimental values in Ref. [1] – the soft-pole PSF shape was assumed there – and those in our model combinations of the B family. As a consequence the predicted Γ_γ for model combinations B, B^*, $B^\dagger$ and $B^\#$ are significantly smaller than the experimental value. This difference indicates that the absolute normalization of Oslo PSF data, shown in Fig. 3, is not fully justified. Normalization using the PSF shapes given by model combinations of the B family to $\Gamma_\gamma^{(exp)}$ would shift the plotted Oslo data significantly higher, bringing them much closer to the (γ,γ') data; a factor of about 1.5 would be needed to match the most probable experimental value. Such a change of normalization would influence the relative size of the enhancement in the model combination $B^\#$ as the absolute value of the low-energy $M1$ is to be independent of any normalization. But as mentioned In Sec. V an allowed change in normalization of the $E1$ PSF would not bring the prediction of MSC spectra with model $B^\#$ to agreement with experimental data.

On the other hand, the predicted Γ_γ with model combinations C^*, D, and to a lesser degree E, are already too high to reproduce $\Gamma_\gamma^{(exp)}$. Values of Γ_γ for model combinations of the A family are in an acceptable agreement with experiment. A multiplication of the absolute values of all PSFs by a factor up to about 1.6 would be still acceptable at the two standard deviation level.

C. Primary transitions from (n,γ) reaction

The f_{E1} PSF determined from the intensities of primary transitions from individual neutron resonances for four nuclei in the Mo mass region were compiled in Ref. [45] and listed in Tab. IV. There are two quantities needed for the determination of f_{E1} from experimental data in this case: (i) the average partial radiation width of primary transitions and (ii) the density of neutron resonances with a given J and π. We found that values of the s-wave resonance spacing D_0 used in Ref. [45] are often substantially smaller than the values proposed later [25, 26]. The recalculated f_{E1} values obtained with the spacing taken from [26] are presented in Tab. IV and Fig. 3. The value of D_0 reported in [25] is usually slightly smaller, but still compatible with that in [26]. No correction for possible non-statistical effects was applied to the data presented; a correction for some of the points is proposed in [45]. The original f_{E1} values from [45] are

		original [45]		recalculated	
Nucleus	E_γ	$\langle D_0\rangle$	$f_{E1}\times10^{-8}$	$\langle D_0\rangle$	$f_{E1}\times10^{-8}$
	(MeV)	(eV)	(MeV^{-3})	(eV)	(MeV^{-3})
^{93}Mo	6.6	1000	5.67(147)	2800(485)	2.02(52)
^{95}Mo	7.3	975	5.38(41)	1690(390)	3.10(24)
^{99}Mo	5.5	429	4.32(81)	970(200)	1.91(36)
^{94}Nb	6.5	37.8	5.04(124)	84.8(46)	2.25(55)
^{100}Ru	6.9	31.4	2.97(41)	21.7(23)	4.30(60)

TABLE IV: The f_{E1} deduced from intensities of primary transitions in (n,γ) reactions. Original f_{E1} values from [45] are given together with recalculated values obtained with help of s-wave resonance spacings D_0 from [26]. No error was added to the recalculated f_{E1} due to uncertainty in the resonance spacings listed in [26].

in very good agreement with the HIγS data, while the recalculated ones agree well with the Oslo data.

The $M1$ strength must be added to the $E1$ strength in order to obtain the "total PSF" to which all other experimental data in Fig. 3 correspond. The f_{M1} from the intensities of primary transitions in [45] in this mass region is about 4- to 8-times smaller than the f_{E1} at $E_\gamma \approx 6-7$ MeV. This f_{E1}/f_{M1} ratio is consistent with that used in all of our simulations and corresponds to a weak $M1$ observed at these E_γ from HIγS (γ,γ') measurement [11].

In practice we do not know the actual D_0 of nuclei listed in Tab. IV, but its value in ^{95}Mo according to Ref. [26] appears in agreement with observations in our recent work [35]. As a result the uncertainty in D_0 makes the data from primaries from radiative neutron capture not very helpful for constraining the PSF models.

VII. CONCLUSIONS ON PSFs IN ^{98}MO

Examining Fig. 3 it seems extremely difficult to reproduce all of the above-mentioned experimental data from (n,γ), (γ,γ'), and ^{3}He-induced reactions with universal PSFs. But despite the huge differences in the experimental data, such universal PSFs might still exist and follow the HIγS data at $E_\gamma > 5$ MeV.

As is evident from the discussion of Γ_γ, the absolute values of PSFs from Oslo data might be incorrect – multiplication of Oslo data from Fig. 3 by a factor of about $1.3-1.8$ is required to reproduce $\Gamma_\gamma^{(exp)}$ within one standard deviation. An even higher multiplication factor would be needed if the NLD deviated significantly from the BSFG model. A multiplication factor of about 2 would then be required to bring the Oslo data in agreement with the HIγS data.

As indicated in Ref. [46], the efficiency corrected ELBE experimental spectra seem to be reasonably consistent with γ-ray spectra coming directly from DICEBOX simulations with no pygmy dipole resonance, i.e., a resonance structure in f_{E1} at $E_\gamma \approx 6$ MeV. This finding might indicate that the "iterative" method used in Ref. [9] for extraction of PSFs from experimental data does not yield unique results and that the ELBE data are in fact consistent with the HIγS data. But additional tests of the method used for processing of ELBE data are necessary.

We would also like to remind here that analysis of only MSC spectra does not allow one to say anything about the absolute values of PSFs. Such analysis is sensitive only to the energy dependence of PSFs and their ratios for different transition types. We observe that a multiplication of PSFs in model combination A by a factor of about 2, which would make the PSFs in this combination consistent with HIγS data, results in overestimation of Γ_γ. This deficiency might be overcome by using (i) a NLD model deviating from BSFG model or (ii) PSFs models with the E_γ dependence slightly differing from that in model combination A. Our attempts to reproduce MSC spectra with a corresponding modification of PSF models were not successful, leaving option (i) as the only possible explanation. We should stress here that the value of Γ_γ from ^{95}Mo(n,γ) reaction predicted with the model combination A, reproducing MSC spectra in ^{96}Mo was fully consistent with the well known value of $\Gamma_\gamma^{(exp)} = 162(7)$ in this nucleus [7].

On the other hand, there exists an alternative explanation of differences in the experimental data from Fig. 3. Analysis of several recently measured (γ,γ') data [11, 47, 48], including that on ^{94}Mo [11], indicated that the γ decay of 1^- excited states at excitation energies of about $5-8$ MeV – i.e., in the region where the PDR is expected – might not be fully governed by the statistical model. More precisely, the validity of the Brink hypothesis was put in question. These (γ,γ') data indicated that contrary to the GEDR and the scissors mode, the PDR could significantly violate the Brink hypothesis and very likely influences only direct transitions to the ground state. In such a case the cross section measured in (γ,γ') would not completely correspond to the PSFs deduced from reactions probing only decay of the highly-excited nucleus. A study of the PDR properties, especially its possible presence in transitions between excited states, is thus of high importance, albeit very difficult as the contribution of decay of states in the PDR region excited in (γ,γ') experiment to spectra measured in other reactions is negligible.

To reproduce the experimental data from the (γ,γ') measurement at 3.75 MeV and also perhaps the behavior of the Oslo and DANCE data below $E_\gamma = 4$ MeV, a temperature-dependent PSF model would probably be required. The T-dependence, not necessarily the same as of the GLO model, could be responsible for an enhancement of Oslo PSFs at low E_γ. Very detailed tests of the influence of the temperature dependence of PSF on Oslo data, similar to those reported in [49], for Mo nuclei would be needed.

In any case, our understanding of γ decay of nuclei in Mo mass region is far from desired and further effort in both experiment and theory is needed.

VIII. SUMMARY

Measurement of the multi-step γ cascades following neutron resonance capture in an isotopically enriched ^{97}Mo sample was performed with the DANCE detector array using the time-of-flight method.

The multiplicity distribution of the detected γ cascades in combination with the spectral shapes of the MSC γ-ray spectra placed spin restrictions on almost all of the neutron resonances observed in our experiment at energies below 1.7 keV. A unique spin assignment could be made for about half of them.

The MSC γ-ray spectra for different multiplicities from resonances with different spins and parities were used to test the validity of various PSF models in ^{98}Mo. The MSC spectra for ^{98}Mo seem to be well described with a PSF model combination reproducing MSC and TSC spectra for the neighboring nucleus ^{96}Mo, a combination which incorporates the Generalized Lorentzian model for $E1$ transitions, the $M1$ spin-flip resonance and a weak single-particle component of the $M1$ photon strength. Our data also indicate that no pronounced resonance structure such as that reported previously near 2 MeV from the ^{3}He-induced reaction [1] or near 6 MeV from the Dresden (γ, γ') measurement [9] or a low-energy enhancement comparable to that predicted by shell-model calculations [4] can be present in a (temperature-independent) PSF model.

Our discussion of the consistency of PSF models deduced from analysis of MSC spectra with data from other experiments in Mo region clearly indicates a huge difficulty in obtaining a universal PSF model combination that would reproduce all available experimental data in the Mo nuclei. A violation of Brink hypothesis by the pygmy dipole resonances is proposed as a tentative explanation of the differences between experimental data from different experiments. Further investigation of PSFs in this region is highly required.

Acknowledgments

This work was supported in part by the U. S. Department of Energy Grants No. DE-NA0001784 and No. DE-FG02-97-ER41042. This work benefited from the use of the LANSCE accelerator and was performed under the auspices of the U. S. Department of Energy at Los Alamos National Laboratory by the Los Alamos National Security, LLC under contract No. DE-AC52-06NA25396 and LLNL contract No. DE-AC52-07NA27344. It was also supported by grant No. 13-07117S of the Czech Science Foundation.

[1] M. Guttormsen *et al.*, Phys. Rev. C **71**, 044307 (2005).
[2] M. Wiedeking *et al.*, Phys. Rev. Lett. **108**, 162503 (2012)
[3] E. Litvinova, N. Belov, Phys. Rev. C **88**, 031302 (2013).
[4] R. Schwengner, S. Frauendorf, A.C. Larsen, Phys. Rev. Lett. **111**, 232504 (2013)
[5] B.A. Brown, A.C. Larsen, Phys. Rev. Lett. **113**, 252502 (2014)
[6] M. Krtička *et al.* Phys. Rev. C **77**, 054319 (2008).
[7] S.A. Sheets *et al.* Phys. Rev. C **79**, 024301 (2009).
[8] G. Rusev *et al.*, Phys. Rev. C **73**, 044308 (2006).
[9] G.Rusev *et al.*, Phys. Rev.C **77**, 064321 (2008).
[10] G. Rusev *et al.*, Application of Accelerators in Research and Industry: 20^{th} International Conference, AIP 1099, 799 (2009).
[11] C. Romig *et al.*, Phys. Rev. C **88**, 044331 (2013).
[12] M. Heil et al., Nucl. Instrum. Methods Phys. Res. A **459**, 229 (2001).
[13] R. Reifarth *et al.*, Nucl. Instrum. Methods Phys. Res. A **531**, 530 (2004).
[14] P. W. Lisowski and K. F. Schoenberg, Nucl. Instrum. Methods Phys. Res. A **562**, 910 (2006).
[15] M. Mocko and G. Muhrer, Nucl. Instrum. Methods Phys. Res. A **704**, 27 (2013).
[16] M. Jandel *et al.*, Phys. Rev. C **78**, 034609 (2008).
[17] J. M. Wouters et al., IEEE Trans. Nucl. Sci. **53**, 880 (2006).
[18] F. Bečvář, Nucl. Instrum. Methods Phys. Res. A **17**, 434 (1998).
[19] C.E. Porter and R.G. Thomas, Phys. Rev. **104**, 483 (1956).
[20] M. Jandel *et al.*, Nucl. Instrum. Methods Phys. Res. B **261**, 1117 (2007).
[21] Balraj Singh, Zhiqiang Hu, Nuclear Data Sheets **98**, 335 (2003); www.nndc.bnl.gov/ensdf
[22] T. von Egidy and D. Bucurescu, Phys. Rev. C **72**, 044311 (2005).
[23] T. von Egidy and D. Bucurescu, Phys. Rev. C **80**, 054310 (2009).
[24] R. Chankova *et al.*, Phys. Rev. C **73**, 034311 (2006)
[25] R. Capote *et al.*, Nucl. Data Sheets **110**, 3107 (2009).
[26] S. F. Mughabghab, *Atlas of Neutron Resonances* (Elsevier, Amsterdam, 2006).
[27] S.I. Al-Quraishi *et al.*, Phys. Rev. C **67**, 015803 (2003).
[28] J. Kopecky and M. Uhl, Phys. Rev. C **41**, 1941 (1990), and references therein.
[29] D.M. Brink, Ph.D. thesis, Oxford University (1955).
[30] H. Beil *et al.* Nucl. Phys. A **227**, 427 (1974).
[31] B.L. Berman *et al.*, Phys. Rev. C **36**, 1286 (1987).
[32] H. Utsunomiya *et al.*, Phys. Rev. C **88**, 015805 (2013)
[33] A. Schiller *et al.*, Nucl. Instrum. Methods Phys. Res. A **447**, 498 (2000).
[34] G. A. Bartholomew *et al.*, Adv. Nucl. Phys. **7**, 229 (1973).
[35] S.A. Sheets *et al.* Phys. Rev. C **76**, 064317 (2007).
[36] F. Bečvář *et al.*, Nucl. Instrum. Methods Phys. Res. A

647, 73 (2011).
[37] A. Chyzh *et al.* Phys. Rev. C **84**, 014306 (2011).
[38] B. Baramsai *et al.* Phys. Rev. C **85**, 024622 (2012).
[39] https://www.oecd-nea.org/dbdata/jeff/
[40] K. Shibata *et al.*, J. Nucl. Sci. Technol. **48(1)**, 1 (2011); http://wwwndc.jaea.go.jp/jendl/j40/j40.html
[41] S.F. Mughabghab *et al.*, Phys. Rev. Lett. **36**, 1118 (1971).
[42] A.R. De L. Musgrove *et al.*, Nucl. Phys. **A270**, 108 (1976).
[43] P.E. Koehler *et al.*, Phys. Rev. C **88**, 041305 (2013).
[44] N. Lo Iudice and F. Palumbo, Phys. Rev. Lett. 41, 1532 (1978).
[45] J. Kopecky, M. Uhl, contribution to the NEA/ENEA and IAEA specialists' meating on measurement, calculation and evaluation of photon production data, Bologna, Italy, Nov. 9-17, 1994.
[46] M. Krtička and F. Becvář, EPJ Web of Conferences 2, 03002 (2010)
[47] C.T. Angell *et al.*, Phys. Rev. C **86**, 051302 (2012).
[48] J. Isaak *et al.*, Phys. Lett. **B727**, 361 (2013).
[49] A.C. Larsen *et al.*, Phys.Rev.C **83**, 034315 (2011).